doi: 10.22564/rbgf.v9i1.1101

# LOW-LATITUDE IONOSPHERIC DYNAMICAL PROCESSES FROM ATOMIC OXYGEN NIGHTGLOW EMISSIONS

J.A. BITTENCOURT & Y. SAHAI

Simultaneous observations of permitted and forbidden atomic oxygen airglow emissions have been used in the past by several investigators to study nighttime dynamical processes in the low-latitude F-region ionospheric plasma. Simultaneous measurements of the emissions OI 135.6 nm (or OI 777.4 nm) and OI 630.0 nm, either from satellite or from ground-based instrumentation, can be used to infer the F-region peak electron density, $n_m(e)$, and height, $h_m$. Results are presented showing the use of this remote sensing technique to study low-latitude ionospheric dynamical processes, including mapping of F-region plasma irregularities and transequatorial plasma bubbles, ionospheric effects due to thermospheric neutral winds and ionospheric response during magnetically disturbed conditions.

PROCESSOS DINÂMICOS DA IONOSFERA EM LATITUDES BAIXAS A PARTIR DE EMISSÕES LUMINESCENTES DO OXIGÊNIO ATÔMICO – Observações simultâneas das emissões de luminescência atmosférica do oxigênio atômico têm sido utilizadas no passado por vários pesquisadores para estudar os processos dinâmicos da região F do plasma ionosférico em baixas latitudes. Medidas simultâneas das emissões OI 135,6 nm (ou OI 777,4 nm) e OI 630,0 nm, a partir de satélites ou instrumentação de solo, podem ser usadas para inferir a densidade eletrônica do pico, $n_m(e)$, e a altura do pico, $h_m$, da região F. Resultados são apresentados ilustrando o uso desta técnica de sensoriamento remoto para estudar os processos dinâmicos da ionosfera de baixa latitude, incluindo mapeamento das irregularidades de plasma na região F e bolhas de plasma transequatoriais, efeitos ionosféricos devidos a ventos neutros termosféricos e resposta ionosférica durante condições de distúrbios magnéticos.

## INTRODUCTION

Dynamical transport processes play an important role in determining the tropical ionospheric F-layer ionization distribution around the magnetic equator. Two regions of enhanced plasma concentration are known to be produced at about 15° on either side of the magnetic equator, with significant local time and seasonal variations (see, e.g. Lyon & Thomas, 1963; Hanson & Moffett, 1966; Anderson 1973a, b; Matuura, 1979). This very nonuniform latitudinal ionization distribution, known as the Appleton or ionospheric equatorial anomaly, is mainly the result of the three transport processes, which concentrate the ionization in regions other than that of its production: (1) plasma diffusion along the magnetic field lines, due to pressure gradients and gravity; (2) electromagnetic **E** x **B** plasma drift, due to an east-west electric field, which moves the ionization perpendicularly to the magnetic field lines in the well-known fountain effect, producing two symmetrical regions of enhanced plasma density about the magnetic equator; and (3) thermospheric neutral wind drag, which transports the ionization in the direction of the wind velocity component along the field line. The latter process produces, in general, an asymmetrical distribution of ionization about the magnetic equator, with different values of the F-region peak electron density, $n_m(e)$, and peak height, $h_m$, at the ionization crests about 15° either side of the dip equator (Bramley & Young, 1968; Abur-Robb & Windle, 1969).

Associated with this asymmetrical ionization distribution about the dip equator, there is an asymmetrical intensity distribution of atomic oxygen tropical airglow emissions which arise from ionization recombination mechanisms. The tropical atomic oxygen nightglow emissions at, e.g., 135.6 nm, 130.4 nm, 777.4 nm and 630.0 nm, are well known to occur in the form of two bands or arcs of enhanced emissions at about 15° on either side of the magnetic dip equator, showing great similarity with the ionospheric F-region equatorial anomaly (King, 1968; Hicks & Chubb, 1970; Reed et al., 1973; Bittencourt & Tinsley, 1976).

The two mechanism responsible for the tropical

Instituto de Pesquisas Espaciais - INPE, Caixa Postal 515, 12201 São José dos Campos, São Paulo, Brasil.

nightglow emissions at 135.6 nm, 130.4 nm and 777.4 nm are radiative recombination of $O^+$ ions (Hanson, 1969; Tinsley et al., 1973) and to a smaller extent, oxygen ion-ion mutual neutralization (Knudsen, 1970). The tropical 630.0 nm nightglow emission is known to be produced almost exclusively by the dissociative recombination of $O_2^+$ ions (e.g., Peterson et al., 1966). This process was first suggested as a source of the 630.0 nm airglow by Bates (1946). As discussed by Tinsley & Bittencourt (1975) (see, also, Sahai et al., 1981a), atomic oxygen airglow emissions (such as 135.6 nm and 777.4 nm) arising mainly from radiative recombination of $O^+$ ions in the F-region provide an indirect measurement of the F-region peak electron density, $n_m(e)$, and simultaneously with the 630.0 nm emission, can be used to infer the F-region peak height, $h_m$. The 630.0 nm emission rate is greater on the F-layer bottomside and its intensity is greatly dependent on the ionospheric vertical motions.

Measurements of these atomic oxygen tropical airglow emissions are therefore suitable for remote sensing of the ionospheric F-region plasma parameters $n_m(e)$ and $h_m$, and to study F-region dynamical processes, since $h_m$ is a very sensitive indicator of ionospheric motions. F-layer height differences at low latitude magnetic conjugate points can be used to determine thermospheric neutral wind velocities along the magnetic meridian (see, e.g., Bittencourt & Tinsley, 1976, 1977; Bittencourt et al., 1976; Bittencourt & Sahai, 1978). This technique can also be used to investigate large scale plasma irregularities, such as transequatorial field-aligned plasma bubbles (Sobral et al., 1980b; Moore & Weber, 1981; Sahai et al., 1981b; Tinsley, 1982; Bittencourt et al., 1983), as well as wave phenomena and variations or perturbations in the F-region, such as during magnetic storms (Sobral et al., 1981; Sahai et al., 1988). Scanning measurements of these emissions provide a way of mapping the ionospheric parameters $n_m(e)$ and $h_m$ over a large geographical region of the sky and to determine their spatial structure and time evolution.

In this paper we present experimental observations and results illustrating the use of this remote sensing technique to study low latitude F-region dynamical processes, including mapping of ionospheric plasma irregularities and transequatorial field-aligned plasma bubbles, ionospheric effects due to thermospheric neutral winds and ionospheric response during magnetic disturbances.

## DETERMINATION OF F-REGION PARAMETERS FROM AIRGLOW EMISSIONS

Following the formalism and notation of Tinsley & Bittencourt (1975), the column emission rate, $J_\lambda^r$, due to radiative recombination, can be expressed as

$$J_\lambda^r = \int \alpha_\lambda \, n(O^+) \, n(e) \, dz \tag{1}$$

and the column emission rate, $J_\lambda^i$, due to ion-ion recombination, as

$$J_\lambda^i = \int \frac{\beta_\lambda \, K_1 \, K_2 \, n(O) \, n(O^+) \, n(e) \, dz}{K_2 \, n(O^+) + K_3 \, n(O)} \tag{2}$$

where $\lambda$ stands for the wavelength of either the 135.6 nm or the 777.4 nm OI emission. The column emission rate, $J_\lambda^d$, due to dissociative recombination, is given by

$$J_\lambda^d = \int \frac{K \, A_\lambda \, \gamma_1 \, n(O_2) \, n(O^+) \, dz}{A[1 + d(z)/A]} \tag{3}$$

where here $\lambda$ stands for the 630.0 nm OI emission.

Writing the electron number density n(e) in the form

$$n(e) = n_m(e) \; S(z) \tag{4}$$

where S(z) is a shape function for the electron density profile, such that $S(h_m) = 1$, the total column emission rate due to radiative and ion-ion recombination ($J_\lambda^r + J_\lambda^i$) can be expressed, from eqs. (1) and (2), as

$$J_\lambda = n_m^2(e) \left[ \int \alpha_\lambda \, S^2(z) \, dz + \right.$$

$$\left. + \int \frac{\beta_\lambda \, K_1 \, K_2 \, n(O) \, S^2(z) \, dz}{K_2 \, n_m(e) \, S(z) + K_3 \, n(O)} \right] \tag{5}$$

whereas the column emission rate due to dissociative recombination becomes, from eq. (3),

$$J_\lambda^d = n_m(e) \, \frac{K \, A_\lambda}{A} \int \frac{\gamma_1 \, n(O_2) \, S(z) \, dz}{[1 + d(z)/A] \, [1 + B(z)]} \tag{6}$$

As discussed by Tinsley & Bittencourt (1975), the contribution from ion-ion recombination is normally a small fraction of that from radiative recombination, and becomes negligible when the F-layer is at high altitude or has high electron density. In any case, from eq. (5) it is seen that $(J_{135.6})^{1/2}$ or $(J_{777.4})^{1/2}$ is proportional to $n_m(e)$ and nearly independent of $h_m$.

Taking the ratio of $J_\lambda^{1/2}$ from eq. (5) (for the 135.6 nm or 777.4 nm OI emissions) to $J_{630.0}$ from eq.

(6), the strong dependence on $n_m(e)$ is conveniently eliminated, so that this ratio becomes a single-valued function of $h_m$ with only a second order dependence on $n_m(e)$, and of course on exospheric temperature also.

Calculations performed for exospheric temperatures of 800 K, 1000 K and 1200 K, using the reaction rate coefficients and atmospheric model as described by Tinsley & Bittencourt (1975) and Sahai et al. (1981a), are presented in Figs. 1 and 2, taken from Sahai et al. (1981a), for the emissions at 777.4 nm and 630.0 nm. It is seen from Fig. 1, that $(J_{777.4})^{1/2}$ is a linear function of $n_m(e)$ with a second order dependence on $h_m$ and exospheric temperature. The dots of Fig. 1 correspond to observed $n_m(e)$ from the ionosonde and observed $(J_{777.4})^{1/2}$, which fits the calculated results reasonably well. It is also seen, from Fig. 2, that the ratio $(J_{777.4})^{1/2}/J_{630.0}$ is a monotonically increasing function on $h_m$ with some dependence on exospheric temperature, and second order dependence on $n_m(e)$. The dots in Fig. 2 correspond to the measured values of $h_m$ from the ionosonde and the observed intensities of $J_{777.4}$ and $J_{630.0}$. The scatter of data points are considered to be due to exospheric temperature changes during the night and from one night to another, since the dots correspond to data obtained for different nights and different local times during a given night.

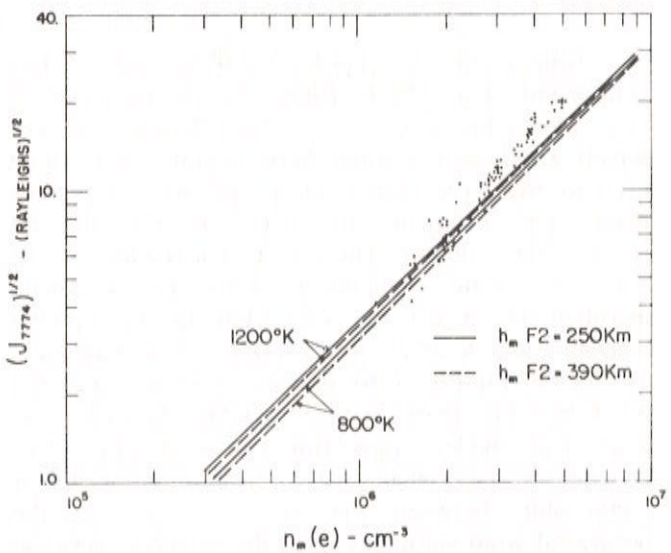


**Figure 1.** Variation of $(J_{777.4})^{1/2}$ with $n_m(e)$ for exospheric temperatures of 800 K and 1200 K and peak heights of 250 km and 390 km. Solid circles are the plots of the observed $(J_{777.4})^{1/2}$ against $n_m(e)$ measured with the ionosonde.

**Figura 1.** Variação de $(J_{777.4})^{1/2}$ com $n_m(e)$ para temperaturas exosféricas de 800 K e 1200 K, e altitudes de pico de 250 km e 390 km. Os círculos sólidos indicam os valores observados de $(J_{777.4})^{1/2}$ contra os valores de $n_m(e)$ medidos com a ionossonda.

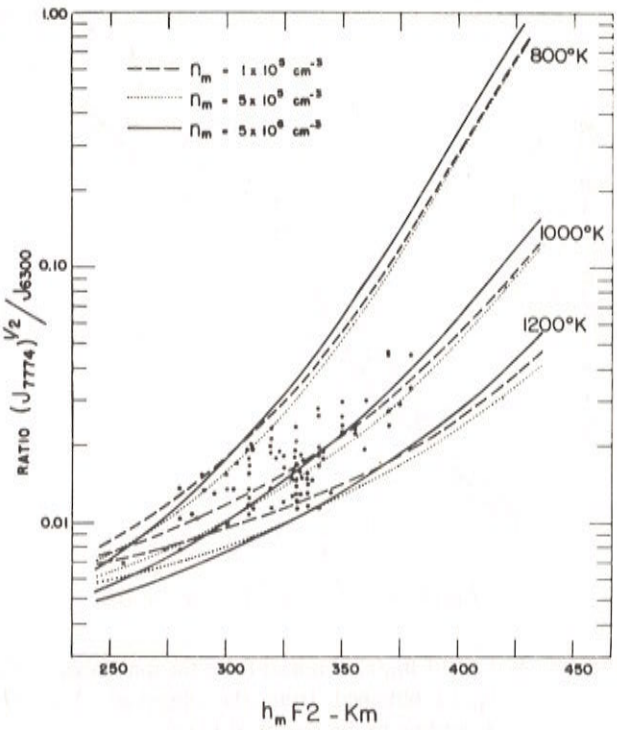


**Figure 2.** Variation of the ratio $(J_{777.4})^{1/2}/J_{630.0}$ with $h_m$ for exospheric temperatures of 800 K, 1000 K and 1200 K, and peak electron densities of 1 x $10^5$, 5 x $10^5$ and 5 x $10^6$ cm$^{-3}$. Solid circles represent the observed ratios $(J_{777.4})^{1/2}/J_{630.0}$ against $h_pF2$ from the ionosonde.

**Figura 2.** Variação da razão $(J_{777.4})^{1/2}/J_{630.0}$ com $h_m$ para temperaturas exosféricas de 800 K, 1000 K e 1200 K, e densidades eletrônicas de pico de 1 x $10^5$, 5 x $10^5$ e 5 x $10^6$ cm$^{-3}$. Os círculos sólidos representam os valores observados da razão $(J_{777.4})^{1/2}/J_{630.0}$ contra os valores de $h_pF2$ medidos com a ionossonda.

For experimental verification of these theoretical calculations we have made a comparison between the F-region parameters $n_m(e)$ and $h_m$ obtained simultaneously from the ionosonde measurements and from the airglow emission intensities. The results for a few nights of observations are show in Figs. 3 and 4, taken from Sahai et al. (1981a). Temperature changes during each night of observation were calculated using the Jacchia 77 atmospheric model (Jacchia, 1977) for that night. The systematic departure from the straight line of 45° slope may be due to calibration uncertainties in the airglow measurements or departures from the assumed Chapman layer shape and other assumptions inherent to the numerical calculations, such as the reaction rate coefficients or the Jacchia atmospheric model. In any case, the near-linear variation of the data indicates the usefulness of the OI emissions to estimate the F-layer peak density and peak height, and to study the variations in these parameters due to ionospheric dynamical processes.

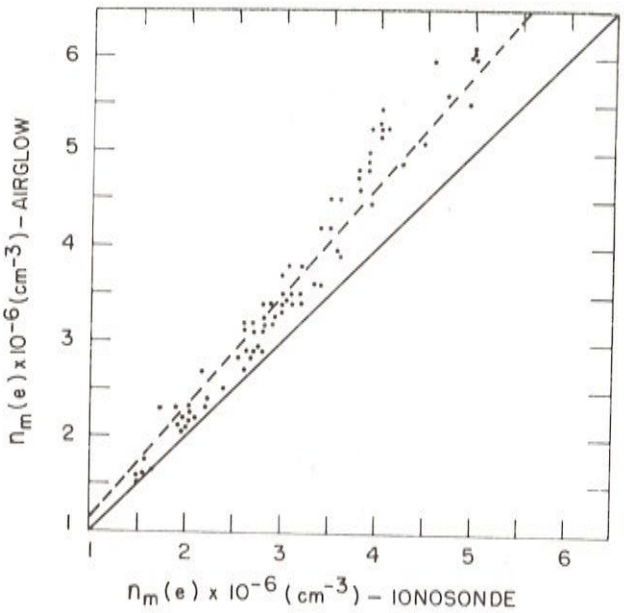


**Figure 3.** Plot of $n_m(e)$ obtained from the ionosonde versus $n_m(e)$ obtained from the observed $(J_{777.4})^{1/2}$ according to the results of Fig. 1.

**Figura 3.** Valores de $n_m(e)$, medidos com a ionossonda, versus $n_m(e)$ obtidos dos valores observados de $(J_{777.4})^{1/2}$, conforme os resultados apresentados na Fig. 1

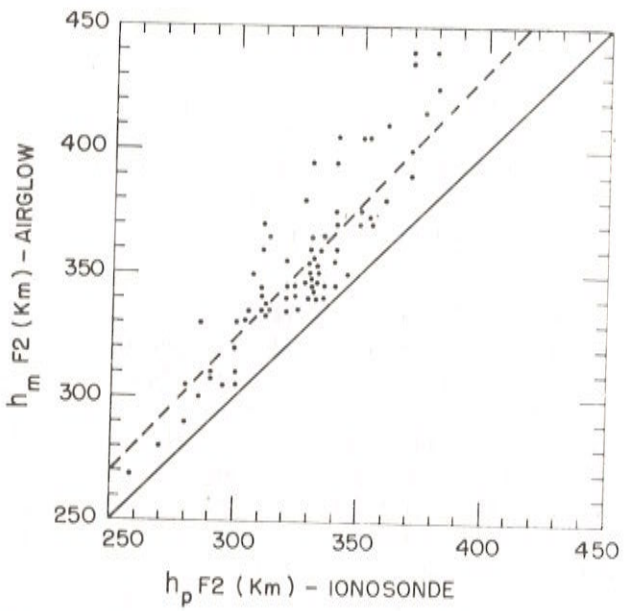


**Figure 4.** Plot of $h_m$ obtained from the ionosonde versus $h_m$ inferred from the observed intensity ratio $(J_{777.4})^{1/2}/J_{630.0}$ according to the results of Fig. 2.

**Figura 4.** Valores de $h_m$, medidos com a ionossonda, versus $h_m$ inferidos a partir das observações da razão de intensidades $(J_{777.4})^{1/2}/J_{630.0}$, conforme os resultados apresentados na Fig. 2

According to the results of Figs. 1 and 3 we obtain the following approximate expression for the F-layer critical frequency, $f_oF2$ (in MHz), in terms of $J_{777.4}$ (in Rayleighs),

$$f_oF2 = (430\ J_{777.4})^{1/4} \tag{7}$$

The critical frequency $f_oF2$ (in MHz) is related to $n_m(e)$ (in $cm^{-3}$) according to the well-known formula,

$$n_m(e) = 1.24 \times 10^4\ (f_oF2) \tag{8}$$

The relationship between $h_m$ and the ratio $(J_{777.4})^{1/2}/J_{630.0}$ is not so simple, but from Fig. 2 it can be seen that the higher this ratio, the higher is $h_m$, the corresponding variation decreasing with exospheric temperature. F-layer height variations due to dynamical effects can nevertheless be accurately determined, in spite of uncertainties concerning neutral atmosphere parameters and second-order effects.

## IONOSPHERIC F-REGION PLASMA DYNAMICS

Bittencourt & Tinsley (1976) (see, also, Bittencourt et al., 1976; Bittencourt & Sahai, 1978) have shown that the height of the F2-peak is a very sensitive indicator of ionospheric motions, and can be used to study the pattern of neutral wind velocities along the magnetic meridian, in the tropical ionospheric F-region. The effect of a transequatorial horizontal wind component along the magnetic meridian is to lift the ionization in the upwind hemispheric side and to lower it in the downwind side, as illustrated in Fig. 5 (for the case of a transequatorial wind blowing from north to south). According to theoretical models (see Bittencourt et al., 1976; Bittencourt & Sahai, 1978), there is a linear relationship between the algebraic sum of the horizontal wind velocities along the magnetic meridian $(U_\theta^N + U_\theta^S)$, taken at magnetic conjugate points, and the corresponding F2-peak height different $(\Delta h_m)$, which can be expressed (at 15° magnetic latitude) as

$$\frac{\Delta h_m}{(U_\theta^N + U_\theta^S)} = 0.60\ \frac{km}{(m/s)} \tag{9}$$

as illustrated in Fig. 6. The effects of electromagnetic vertical plasma drifts on $h_m$ expected to be symmetric about the magnetic equator.

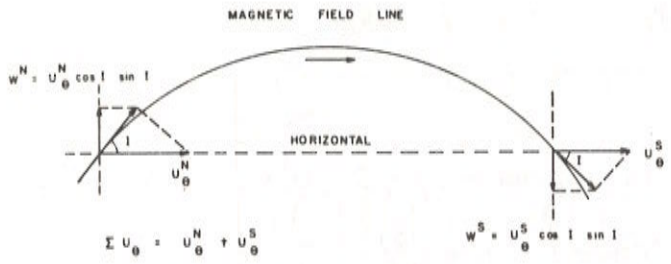


**Figure 5.** Schematic diagram illustrating the vertical ion drift (w) produced by a transequatorial horizontal wind component in the magnetic meridian ($U_\theta$). The dip angle is denoted by I.

**Figura 5.** Diagrama esquemático ilustrando a deriva vertical de ions (w) produzida pela componente ($U_\theta$), ao longo do meridiano magnético, do vento transequatorial horizontal. O ângulo de inclinação magnética está indicado por I.

Using simultaneous measurements of the vertical column emission rates of the OI 135.6 nm and 630.0 nm emissions, made from the OGO 4 satellite, Bittencourt et al. (1976) have inferred the horizontal wind velocity components in the magnetic meridian. Their results are reproduced in Fig. 7, where part (a) shows the velocities determined for the Pacific sector (with magnetic declination, $\delta_m \sim 13^oE$), and part (b) for the Indian sector ($\delta_m \sim 0^o$). The horizontal wind component in the magnetic meridian ($U_\theta$) can be conveniently resolved into geographic zonal ($U'_\phi$) and

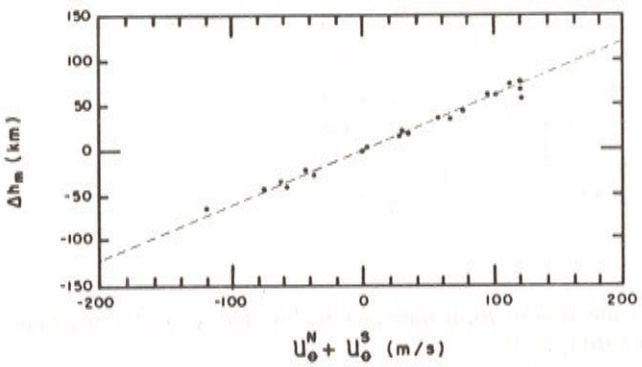


**Figure 6.** Linear relationship between the sum of the horizontal wind velocity component in the magnetic meridian ($U^N_\theta + U^S_\theta$), taken at approximately 15° magnetic latitude, and the corresponding F2-peak height difference ($\Delta h_m$) at the magnetic conjugate points, according to theoretical models.

**Figura 6.** Relação linear entre a soma das componentes da velocidade do vento horizontal ($U^N_\theta + U^S_\theta$), ao longo do meridiano magnético, na latitude magnética em torno de 15°, e a diferença entre as altitudes correspondentes do pico F2 ($\Delta h_m$) nos pontos conjugados magnéticos, conforme os modelos teóricos.

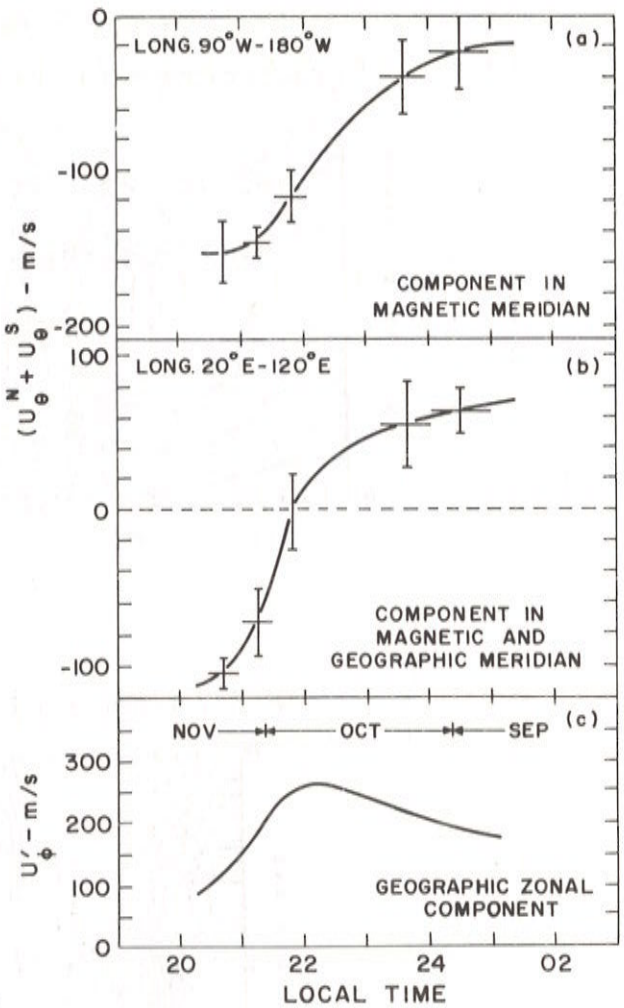


**Figure 7.** Horizontal wind velocities in the magnetic meridian inferred from the OGO 4 satellite airglow observations for (a) the Pacific sector ($\delta_m \sim 13^oE$); (b) the Indian sector ($\delta_m \sim 0^o$). The geographic zonal wind component, deduced from the results presented in (a) and (b), is shown in (c). See text for more details.

**Figura 7.** Velocidades do vento horizontal, ao longo do meridiano magnético, inferidas das observações de luminescência atmosférica pelo satélite OGO4 para (a) setor Pacífico ($\delta_m \sim 13^oE$); (b) setor Indiano ($\delta_m \sim 0^o$). A componente zonal geográfica do vento, deduzida dos resultados apresentados em (a) e (b), está apresentada em (c). Veja o texto para maiores detalhes.

meridional ($U'_\theta$) components according to

$$U_\theta = U'_\theta \cos(\delta_m) + U'_\phi \sin(\delta_m) \qquad (10)$$

For the Indian sector we see therefore that $U_\theta = U'_\theta$. Assuming that the geographic meridional component of the Indian sector can be applied to the Pacific sector, we can determine the geographic zonal wind component ($U'_\phi$) for the Pacific sector, as shown in Fig. 7(c). The magnitude of the inferred neutral

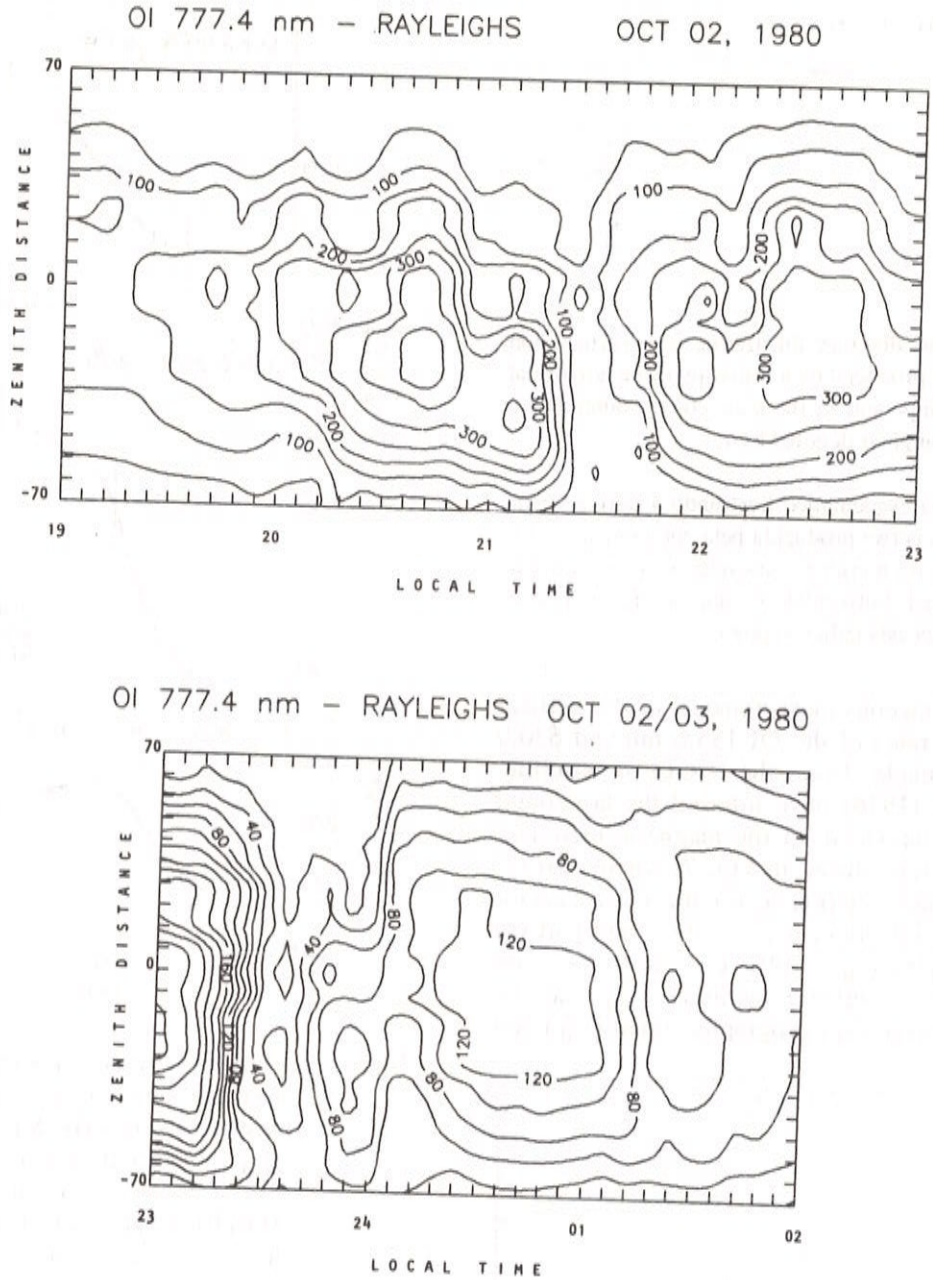


**Figure 8.** Observed intensities for the OI 777.4 nm emission as a function of local time and zenith distance in the magnetic North-South meridian, obtained for the night of October 02/03, 1980.

Figura 8. Intensidades observadas para a emissão OI 777,4 nm em função da hora local e da distância zenital no meridiano magnético Norte-Sul, na noite de 02/03 de outubro de 1980.

wind velocities, the time of occurrence of its maximum and the time of north-south reversal of the meridional components are in good agreement with theoretical wind models at low latitudes (e.g., Geisler, 1967; Kohl & King, 1967; Challinor, 1970; Blum & Harris, 1973). For more details refer to Bittencourt et al. (1976). Wind velocities in the magnetic meridian have also been determined by Bittencourt & Tinsley (1977), and Bittencourt & Sahai (1978), using this approach.

Experimental and theoretical investigations of depleted plasma regions, or ionospheric transequatorial plasma bubbles, and their associated ionospheric irregularities in the tropical ionosphere, have also been made in the past few years, using simultaneous observations of the OI emissions at 777.4 nm and 630.0 nm (see, e.g., Sahai et al., 1981b; Sahai et al., 1983; Bittencourt et al., 1983) and using the OI 630.0 nm emission only (e.g., Weber et al., 1978, 1980;

Sobral et al., 1980a, b, 1981; Mendillo & Baumgardner, 1982). Simultaneous meridional scanning measurements of these emissions have been used by Bittencourt et al. (1983) to construct maps showing the north-south and local time variations of these emissions and the corresponding ionospheric F-region parameters, during quiet and during magnetically disturbed conditions, in the presence of field-aligned large scale plasma irregularities or transequatorial plasma bubbles.

Figures 8 and 9 illustrate the observed intensity variations for the OI 777.4 nm and 630.0 nm emissions, respectively, as a function of local time and zenith distance in the magnetic North-South meridian for the night of October 02/03, 1980, measured at Cachoeira Paulista (geomagnetic latitude 12.0°S; geographic coordinates 22.7°S, 45.0°W). The results are presented in the form of computer generated isointensity contours. Mapping of the associated spatial and temporal variations of $n_m(e)$ and $h_m$ can be obtained, respectively, from $(J_{777.4})^{1/2}$ and the ratio $(J_{777.4})^{1/2}/J_{630.0}$. Large scale field-aligned airglow depletions or patches in both the emissions are seen to be present in these measurements at about 21:30 and 23:30 LT, which are the optical signatures of intertropical transequatorial ionospheric plasma bubbles in the height range of the airglow emissions (Moore & Weber, 1981; Mendillo et al., 1985).

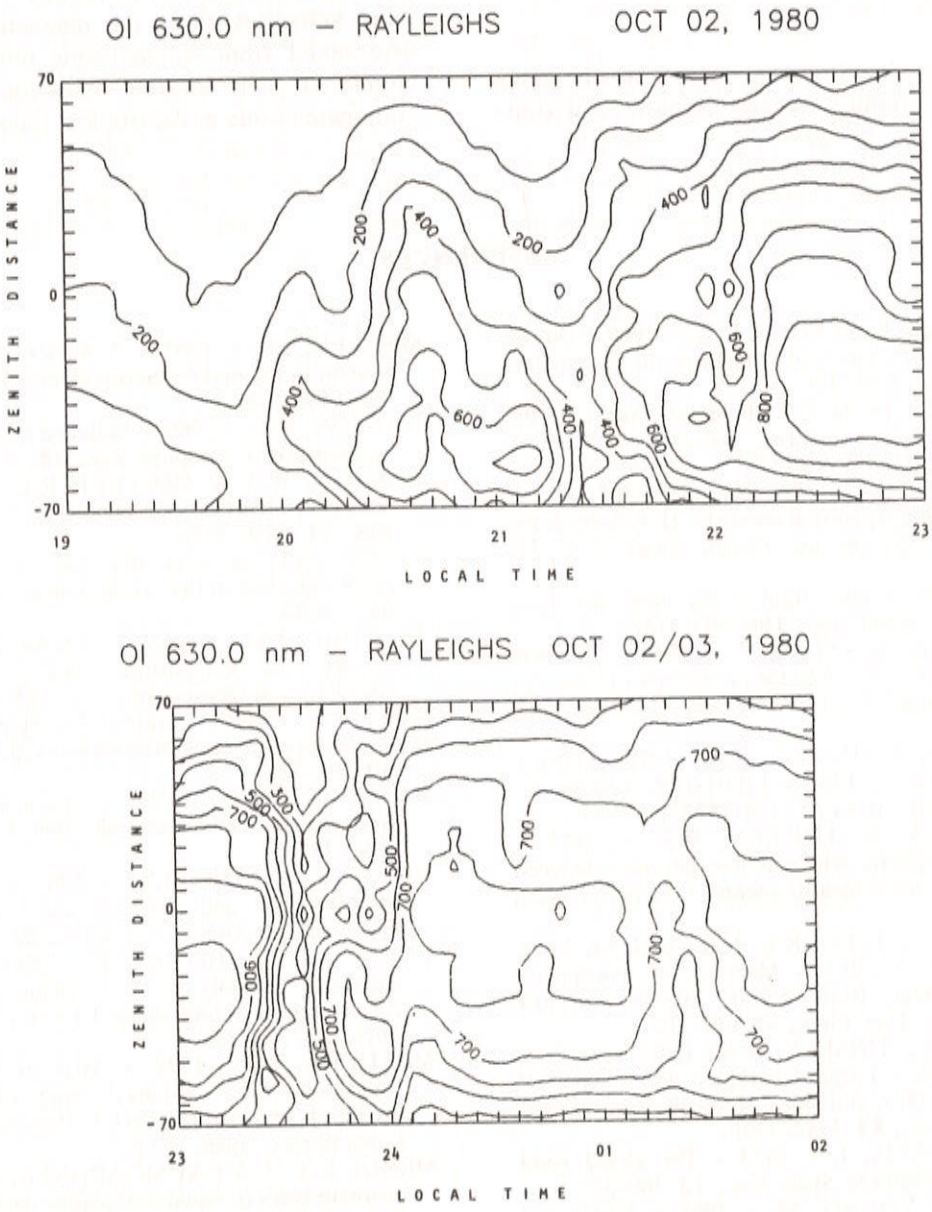


**Figure 9.** Same as in Fig. 8, but for the OI 630.0 nm emission.

**Figura 9.** Idem à Fig. 8, mas para a emissão OI 630,0 nm.

Simultaneous measurements of these atomic oxygen airglow emissions, together with ionosonde measurements and observations of $N_2^+$ particle excited emissions, have been made by Sahai et al. (1988) and used to investigate ionospheric F-region magnetic storm effects at low latitudes. They find that, at low latitudes, there is no significant contribution to the intensity of the OI emissions due to energetic particle precipitation even when there was enhancement in the $N_2^+$ particle excited emissions. Therefore, it seems that the ionospheric recombination mechanisms can quantitatively account for the OI emissions at low latitudes even during strong magnetic storms when $N_2^+$ particle excited emissions are enhanced.

## CONCLUSIONS

This paper has shown that simultaneous measurements of atomic oxygen airglow emissions arising mainly from radiative recombination and from dissociative recombination processes can be used for the remote sensing of the ionospheric F-region plasma parameters $n_m(e)$ and $h_m$. These measurements constitute a very useful and powerful technique to study the dynamical processes in the tropical F-region, where the electron densities are sufficiently high. Scanning measurements or all-sky imaging observations of these emissions provide a good coverage of the spatial and local time variations in $n_m(e)$ and $h_m$. The dynamical evolution of the nighttime tropical ionosphere, including the equatorial Appleton anomaly, wave motions or ionospheric propagating disturbances, and large scale plasma irregularities or transequatorial field-aligned plasma bubbles, can be investigated using this technique. Also, thermospheric wind velocities along the magnetic meridian can be determined from simultaneous observations of these atomic oxygen airglow emissions at magnetically conjugate points in the tropical ionosphere.

## REFERENCES


ABUR-ROBB, M.F.K. & WINDLE, D.W. – 1969 – On the day and night reversal in NmF2 north-south asymmetry. Planet. Space Sci., **17**: 96-106.

ANDERSON, D.N. – 1973a – A theoretical study of the ionospheric F-region equatorial anomaly. I. Theory. Planet. Space Sci., **21**: 409-420.

ANDERSON, D.N. – 1973b – A theoretical study of the ionospheric F-region equatorial anomaly. II. Results in the American and Asian sectors. Planet. Space Sci., **21**: 421-442.

BATES, D.R. – 1946 – The origin of the night sky light. Mon. Notic. Roy. Astron. Soc., **106**: 509-514.

BITTENCOURT, J.A. & SAHAI, Y. – 1978 – F-region neutral winds from ionosonde measurements of hmF2 at low latitude magnetic conjugate regions. J. Atmos. Terr. Phys., **40**: 669-676.

BITTENCOURT, J.A. & TINSLEY, B.A. – 1976 – Tropical F-region winds from OI 1356 and [OI] 6300 A emissions. I. Theory. J. Geophys. Res., **81**: 3781-3785.

BITTENCOURT, J.A. & TINSLEY, B.A. – 1977 – Nighttime thermospheric winds at low latitudes deduced from AE-C ionospheric measurements. J. Geophys. Res., **82**: 4694-4698.

BITTENCOURT, J.A., TEIXEIRA, N.R., SAHAI, Y. & TAKAHASHI, H. – 1983 – Mapping of ionospheric F-region parameters from atomic oxygen airglow emissions. J. Atmos. Terr. Phys., **45**: 697-705.

BITTENCOURT, J.A., TINSLEY, B.A., HICKS, G.T. & REED, E.I. – 1976 – Tropical F-region winds from OI 1356 A and [OI] 6300 A emissions. II. Analysis of OGO-4 data. J. Geophys. Res., **81**: 3786-3790.

BLUM, P.W. & HARRIS, I. – 1973 – The global wind system in the thermosphere. Space Res., **13**: 369-375.

BRAMLEY, E.N. & YOUNG, M. – 1968 – Winds and electromagnetic drifts in the equatorial F-region. J. Atmos. Terr. Phys., **30**: 99-111.

CHALLINOR, R.A. – 1970 – Neutral air winds in the ionospheric F-region for an asymmetric global pressure system. Planet. Space Sci., **18**: 1485-1487.

GEISLER, J.E. – 1967 – A numerical study of the wind system in the middle thermosphere. J. Atmos. Terr. Phys., **29**: 1468-1482.

HANSON, W.B. – 1969 – Radiative recombination of atomic oxygen ions. J. Geophys. Res., **74**: 3720-3722.

HANSON, W.B. & MOFFETT, R.J. – 1966 – Ionization transport effects in the equatorial F-region. J. Geophys. Res., **71**: 5559-5572.

HICKS, G.T. & CHUBB, T.A. – 1970 – Equatorial aurora/airglow in the far ultraviolet. J. Geophys. Res., **75**: 6233-6248.

JACCHIA, L.G. – 1977 – Thermospheric temperature, density and composition: new models. Smithsonian Astrophysical Observatory, Special Report 375.

KING, J.W. – 1968 – Airglow observations and the decay of the ionospheric equatorial anomaly. J. Atmos. Terr. Phys., **30**: 391-402.

KNUDSEN, W.C. – 1970 – Tropical ultraviolet nightglow from oxygen ion-ion neutralization. J. Geophys. Res., **75**: 3862-3866.

KOHL, H. & KING, J.W. – 1967 – Atmosphere winds between 100 and 700 km and their effects on the ionosphere. J. Atmos. Terr. Phys., **29**: 1045-1062.

LYON, A.J. & THOMAS, L. – 1963 – The F2-region equatorial anomaly in the African, American and East Asian sectors during sunspot maximum. J. Atmos. Terr. Phys., **25**: 373-386.

MATUURA, N. – 1979 – Atlas of ionospheric critical frequency ($f_0F2$) obtained from ionosphere sounding satellite-b observation. Part 1. Report of Radio Research Laboratories, Japan, 112 p.

MENDILLO, M. & BAUMGARDNER, J. – 1982 – Airglow characteristics of equatorial plasma depletions. J. Geophys. Res., **87**: 7641-7652.

MENDILLO, M., SPENCE, H. & ZALESAK, S.T. – 1985 – Simulation studies of ionospheric airglow signatures of plasma depletions at the equator. J. Atmos. Terr. Phys., **47**: 885-893.

MOORE, J.G. & WEBER, E.J. – 1981 – OI 6300 and 7774 A

airglow measurements of equatorial plasma depletions. J. Atmos. Terr. Phys., **43**: 851-858.

PETERSON, V.L., VANZANDT, T.E. & NORTON, R.B. – 1966 – F-region nightglow emissions of atomic oxygen. I. Theory. J. Geophys. Res., **71**: 2255-2265.

REED, E.I., FOWLER, W.B. & BLAMONT, J.E. – 1973 – An atlas of low-latitude 6300 A OI night airglow from OGO-4 observations. J. Geophys. Res., **78**: 5658-5675.

SAHAI, Y., BITTENCOURT, J.A., TEIXEIRA, N.R. & TAKAHASHI, H. – 1981a – Simultaneous observations of OI 7774 A and [OI] 6300 A emissions and correlative study with ionospheric parameters. J. Geophys. Res., **86**: 3657-3660.

SAHAI, Y., BITTENCOURT, J.A., TEIXEIRA, N.R. & TAKAHASHI, H. – 1981b – Plasma irregularities in the tropical F-region detected by the OI 7774 A and 6300 A nightglow measurements. J. Geophys. Res., **86**: 3496-3500.

SAHAI, Y., BITTENCOURT, J.A., TEIXEIRA, N.R. & TAKAHASHI, H. – 1983 – Observations of large scale F-region irregularities using airglow emissions at 7774 A and 6300 A. Ann. Geophy., **1**: 271-276.

SAHAI, Y., BITTENCOURT, J.A., TAKAHASHI, H., TEIXEIRA, N.R., SOBRAL, J.H.A., TINSLEY, B.A. & ROHRBAUGH, R.P. – 1988 – Multispectral optical observations of ionospheric F-region storm effects at low latitude. Planet. Space Sci., **36**: 371-381.

SOBRAL, J.H.A., ABDU, M.A. & BATISTA, I.S. – 1980a – Airglow studies on the ionosphere dynamics over low latitude in Brazil. Ann. Geophys., **36**: 199-204.

SOBRAL, J.H.A., ABDU, M.A., BATISTA, I.S. & ZAMLUTTI, C.J. – 1981 – Wave disturbances in the low latitude ionosphere and equatorial ionospheric plasma depletions. J. Geophys. Res., **86**: 1374-1378.

SOBRAL, J.H.A., ABDU, M.A., ZAMLUTTI, C.J. & BATISTA, I.S. – 1980b – Association between plasma bubble irregularities and airglow disturbances over Brazilian low latitudes. Geophys. Res. Letters, **7**: 980-982.

TINSLEY, B.A. – 1982 – Field aligned airglow observations of transequatorial bubbles in the tropical F-region. J. Atmos. Terr., **44**: 547-557.

TINSLEY, B.A. & BITTENCOURT, J.A. – 1975 – Determination of F-region height and peak electron density at night using airglow emissions from atomic oxygen. J. Geophys. Res., **80**: 2333-2337.

TINSLEY. B.A., CHRISTENSEN, A.B., BITTENCOURT, J.A., GOUVEIA, H., ANGREJI, P.D. & TAKAHASHI, H. – 1973 – Excitation of oxygen permitted line emissions in the tropical nightglow. J. Geophys. Res., **78**: 1174-1186.

WEBER, E.J., BUCHAU, J. & MOORE, J.G. – 1980 – Airborne studies of equatorial F-layer ionospheric irregularities. J. Geophys. Res., **85**: 4631-4641.

WEBER, E.J., BUCHAU, J., EATHER, R.H. & MENDE, S.B. – 1978 – North-South aligned equatorial airglow depletions. J. Geophys. Res., **83**: 712-716.

Versão recebida em: 13/02/90
Versão revista e aceita em: 09/01/91
Editor Associado: V.W.J.H. Kirchhoff